BASIC SCIENCE

Nanomedicine: Nanotechnology, Biology, and Medicine
14 (2018) 1371 – 1380

Original Article

nanomedjournal.com

A method for optical imaging and monitoring of the excretion of fluorescent nanocomposites from the body using artificial neural networks

Olga E. Sarmanova[a], Sergey A. Burikov, Ph.D[a,b], Sergey A. Dolenko, Ph.D[b], Igor V. Isaev[a,b], Kirill A. Laptinskiy, Ph.D[a,b], Neeraj Prabhakar, Ph.D[c], Didem Şen Karaman, Ph.D[c], Jessica M. Rosenholm[c], Olga A. Shenderova, Ph.D[d], Tatiana A. Dolenko, Ph.D[a,b,*]

[a]*Lomonosov Moscow State University, Physical Department, Moscow, Russia*
[b]*Skobeltsyn Institute of Nuclear Physics, Lomonosov Moscow State University, Moscow, Russia*
[c]*Pharmaceutical Sciences Laboratory, Faculty of Science and Engineering, Åbo Akademi University, Turku, Finland*
[d]*Adámas Nanotechnologies, Inc., Raleigh, North Carolina, United States*

Received 7 November 2017; accepted 31 March 2018

Abstract

In this study, a new approach to the implementation of optical imaging of fluorescent nanoparticles in a biological medium using artificial neural networks is proposed. The studies were carried out using new synthesized nanocomposites — nanometer graphene oxides, covered by the poly(ethylene imine)-poly(ethylene glycol) copolymer and by the folic acid. We present an example of a successful solution of the problem of monitoring the removal of nanocomposites based on nGO and their components with urine using fluorescent spectroscopy and artificial neural networks. However, the proposed method is applicable for optical imaging of any fluorescent nanoparticles used as theranostic agents in biological tissue.

Key words: Carbon nanocomposite; Fluorescent imaging probe; Fluorescent spectroscopy; Artificial neural networks

According to the International Agency for Research on Cancer GLOBOCAN, in 2012 cancer was diagnosed in 14.1 million people worldwide and the number of deaths from cancer was 8.2 million.[1] The reasons for such high mortality rate are late cancer diagnostics,[2] not so high efficiency of widespread cancer drugs due to their low solubility and poor penetration into tumor cells.[3] These challenges make it necessary to create new agents, mostly based on nanomaterials, that can be used for disease diagnosis and precise identification of tumor localization and also for delivery of drugs attached to nanoparticles to the tumor.[4,5]

The concept of application of both diagnostic and therapeutic nanoagents implies the possibility of tracking their distribution and movement in the body and their removal. Therefore, one of

Abbreviations: ANN, artificial neural network; Cop, copolymer; DLS, dynamic light scattering; FA, folic acid; FRα, alpha receptors for folic acid; MLP, multilayer perceptron; MTX, methotrexate; nGO, nano-graphene oxide; PEG, polyethylene glycol; PEI, polyethyleneimine; TEM, transmission electron microscopy

Support from: This study has been performed at the expense of the grant of Russian Science Foundation (project no. 17-12-01481): O.S., S.B., K.L., T.D.: measurement of sizes and fluorescence quantum yields of nanocomposites, conducting experiments, processing spectra; and at the expense of the grant of Russian Science Foundation (project no. 14-11-00579): I.I., S.D.: data pre-processing, design and methodology of application of ANN. Partial funding from the Academy of Finland (project# 284542, 309374) is also acknowledged (N.P., D.S.K., J.M.R.: synthesis and characterization of nanocomposites).

The authors declare no conflicts of interests.

*Corresponding author at: Physical Department, Lomonosov Moscow State University, Moscow, 119991, Russian Federation.
E-mail addresses: oe.sarmanova@physics.msu.ru (O.E. Sarmanova), sergey.burikov@gmail.com (S.A. Burikov), dolenko@srd.sinp.msu.ru (S.A. Dolenko), isaev_igor@mail.ru (I.V. Isaev), laptinskij@physics.msu.ru (K.A. Laptinskiy), neepra@utu.fi (N. Prabhakar), didem.sen@abo.fi (D.Ş. Karaman), jessica.rosenholm@abo.fi (J.M. Rosenholm), oshenderova@itc-inc.org (O.A. Shenderova), tdolenko@lid.phys.msu.ru tdolenko@mail.ru (T.A. Dolenko).

https://doi.org/10.1016/j.nano.2018.03.009
1549-9634/

Please cite this article as: Sarmanova OE, et al, A method for optical imaging and monitoring of the excretion of fluorescent nanocomposites from the body using artificial neural networks. *Nanomedicine: NBM* 2018;14:1371-1380, https://doi.org/10.1016/j.nano.2018.03.009

the main tasks of nanomedicine is the development of sensitive methods for the imaging of nanoagents in biological tissues.

Nowadays a number of methods for nanoparticles visualization have been developed. These include various types of tomography,[6] gamma scintigraphy,[7,8] magnetic resonance imaging,[7–9] and optical imaging.[7,10] The presence of ionizing radiation, low sensitivity to the number of inserted markers and high cost are essential disadvantages of tomography and gamma scintigraphy.[10] Meanwhile, optical imaging is a highly sensitive and relatively cheap technique.[7,10] Currently, optical imaging is one of the most common techniques in medical imaging.

Optical imaging of nanoparticles is based on the use of their optical properties, primarily luminescent ones. Therefore, special attention is paid to the development of nanoagents that have intense and stable luminescent properties or constructs possessing these properties. To date a large set of nanoparticles possessing intense and stable luminescence that are biocompatible and non-toxic to varying degrees has been developed, which provides ample opportunities to use them as luminescent imaging probes and drug carriers.[11–17] The optimal method of biovisualization of such particles is their recognition by the luminescence spectra.[18] However, background fluorescence, or autofluorescence, caused by the fluorescence of intrinsic fluorophores of biological tissues, is a major problem in the implementation of optical imaging. The spectrum of autofluorescence is in the range from 250 nm to 700 nm and is the result of superposition of fluorescence bands of a large number of such tissue fluorophores as tryptophan, phenylalanine, tyrosine, collagen, etc.[19] Unfortunately, the luminescence bands of almost all medicine nanoparticles overlap with the autofluorescence band, which makes it very difficult to observe them *in vivo* and *in vitro*. Therefore, it is very important to develop a method for separating the luminescent signal of nanoparticles from the autofluorescence of biological tissues and to control its changes to ensure the tracking of the probes.

There are two methods for controlling autofluorescence. The first method involves the creation of new imaging probes, whose luminescence band weakly overlaps with autofluorescnece. The second one involves the development of experimental methods that make it possible to reduce the background of fluorescence. So, at the present time, organic dyes,[10] gold nanoclusters[16] emitting in the near infrared range are being developed. However, new dyes are still insoluble in water and have low quantum yield and low photostability,[20] Due to the quantum-size effect it was possible to obtain semiconductor quantum dots emitting in the range from UV to IR regions of the spectrum.[21] Nevertheless, the problem of semiconductor quantum dots toxicity remains unsolved.[16] Other studies are actively performed to synthesize nanodiamonds doped with silicon: they have a narrow band of fluorescence with a maximum near 738 nm.[22] Thus, despite significant progress in the synthesis of new nanoparticles for biological applications, the problem of optimizing their properties for reliable imaging is far from being solved today.

From the technical point of view, optical microscopy is the basis of most optical methods for imaging agents: laser scanning confocal microscopy,[23] multiphoton microscopy,[24] time-resolved microscopy,[25] photoacoustic imaging with a high resolution.[26]

When developing imaging probes, attention should also be paid to controlling the excretion of nanoparticles from the body. For this purpose, medical research uses various methods for estimating the amount of extracted nanoparticles, such as radioactive labeling,[27] direct neutron irradiation,[28] etc. For instance, flow cytometers measure the fluorescence intensity and determine the number of fluorescently-marked objects passing through the analyzed volume in the liquid flow.[29] All these methods are quite effective, but they require expensive equipment.

Together with the technical capabilities, the methods of processing image information are also actively developing. In the study[30] structured illumination microscopy allowed obtaining a resolution of 50 nm. At present, three-dimensional methods of tracking single particles in biological tissue are elaborated.[31–34]

Nowadays, methods involving artificial neural networks (ANN) are actively developing.[35] ANNs represent powerful data analysis algorithms that provide effective solution of inverse and pattern recognition problems in optical spectroscopy,[35–42] in many fields of biology and medicine.[36] Currently the solution of problems such as classification of proteins, detachment of fragments of the genome, recognition of signal peptides, etc.[37] with ANN is very promising. The authors in Ref.[38] proposed a method for the diagnosis of breast cancer, in which ANN solved the problem of distinguishing healthy cell cultures and cancer cells by their spectra of autofluorescence. Authors in Ref.[43] try to predict drug-carrier size on the basis of the weight ratio of the carrier and the drug using probabilistic ANNs. Authors of the study[44] predict the level of cytotoxicity of the nanocomposite by its size. In Ref.[45] genetic variation was determined from the mass spectra of biological tissues incubated with gold nanoparticles using ANNs.

In this study we propose a new approach to solving the problem of optical imaging of luminescent nanoparticles in biological medium on the example of monitoring of the removal of fluorescent nanocomposites based on carbon dots and their components with urine using ANNs. Due to various interactions between biomacromolecules and nanoparticles, which result in alterations of nanoparticles autofluorescence and luminescence signal, and also due to high variability of biological tissue fluorescence, extraction of individual fluorescence signals of nanoparticles and biological tissue from their common spectrum using traditional methods seems almost impossible. The general advantage of ANN application in this case is the fact that neural network is trained on experimental examples directly — fluorescence spectra of all types: biological tissues without nanoparticles, nanoparticles outside biological tissues, and fluorescence spectra of biological objects with nanoparticles of different concentrations. Due to such training ANN is able to learn how to approximate the changes in the spectra, which are due to the variability of autofluorescence and interactions between the surface of nanoparticles and biological tissue. All these ensure not only the recognition of fluorescence signals of nanoparticles on the background of autofluorescence, but also the determination of nanoparticles concentration in a biological medium.

Despite the extremely wide application of machine learning methods in biomedicine, we do not possess any information about any studies, where these methods were applied for optical imaging of nanoparticles in a medium of biological origin. Earlier we demonstrated the fundamental possibility of optical monitoring of carbon nanoparticles in biological tissues using neural network algorithms. The problem of identification and determination of the concentration of fluorescent nanodiamond imaging probes against chicken protein[46] and urine[47] using ANN was successfully solved. In this study, the possibility of optical imaging of carbon nanoparticles is confirmed, and a complex multi-parametric problem of optical imaging of nanoparticles in a biological medium is solved: using ANN it is determined which nanoparticles – the nanocomposite itself and/or its components – and in what quantities, these are present in human urine.

Methods

Materials characterization

Graphene oxide nanoparticles (nGO) are products of the chemical reactions of intercalation, delamination and oxidation of 400 nm nanographite plates (Nanostructured&Amorphous Materials Inc., Houston, TX) in a 3:1 mixture of sulfuric and nitric acids.[48] After evaporation of the acids from the supernatant (at 350°C), the nGO pellet was washed and dispersed in deionized water.

mPEG (molecular weight 5000), PEI (molecular weight 25000), hexamethylene diisocyanate (> 99%), folic acid ligands (FA, >99%) from Sigma Aldrich were used for the synthesis of the copolymer with folic acid. During the process of conjugation of the copolymer (Cop) and FA, polyethylene glycol maleimide (malPEG-OH, molar mass PEG 5 K), prepared according to JENKEM technology, was used as the initial reagent. During the synthesis of nanocomposites, organic solvents, anhydrous chloroform and diethyl ether were used from Riedel-de Haën and J.T.Baker, respectively, and Milli-Q water (18.2 MΩ). The synthesis of the copolymer and the process of coating of the nGO copolymer are described in detail in Ref.[14]

Human urine was selected as a biological medium from three different donors aged 18 to 25 years.

Characterization of nGO, nGO+Cop and nGO+Cop+FA nanocomposites in HEPES buffer (25 mM, pH = 7.2) was carried out: their sizes and zeta potentials were measured; luminescent properties of aqueous suspensions of nGO, nGO+Cop and nGO +Cop+FA, biocompatibility and non-toxicity of nanomaterials were tested.[14]

Measurements of nanocomposite sizes in aqueous suspensions using dynamic light scattering (DLS) were carried out on a correlator-goniometric system ALV-CGS-5000/6010 (Langen, Germany) equipped with a He-Ne laser (wavelength 632.8 nm, power 20 mW).

The zeta potentials were measured on a Malvern Zetasizer instrument (Model Nano ZS, Malvern, Worcestershire, UK).

Luminescence signal and Raman scattering of the nanoparticle suspensions were excited by a diode laser (wavelength 405 nm, power 50 mW). As a recording system, the Thorlabs CCS200 spectrometer was used. Practical resolution was 2 nm. The thermal stabilization system allows to control the sample temperature with an accuracy of 0.2°C. The spectra were normalized to the power of laser radiation and to the spectrum accumulation time.

The absorption spectra of the samples were recorded on a Perkin Elmer Lambda 25 spectrophotometer.

Fluorescence quantum yields of nanoparticles in aqueous suspensions were calculated by the formula:

$$\varphi_2 = \frac{S_2}{S_1} * \frac{D_1}{D_2} * \varphi_1,$$

where S_2 and S_1 are the areas under the fluorescence curves of the investigated and reference substances, D_2 and D_1 are the values of the optical absorption coefficient of the investigated and reference substances at the excitation wavelength, φ_2 and φ_1 are the fluorescence quantum yields of the investigated and reference substances. As a standard, a solution of the Rhodamine 6G in ethanol (concentration 10^{-6} M) was used, the quantum yield of which is equal to 0.95 according to the data of Ref.[49]

The visualization of nGO+Cop+FA nanocomposites (10 μg/mL) in HeLa cancer cells was carried out using a fluorescent confocal microscope (TCS SP 5, Leica Microsystems, Germany, exc. 488 nm).

Artificial Neural Networks

ANN is a class of mathematical methods that have demonstrated high efficiency in solving problems of data mining — approximation, prediction, estimation, classification and pattern recognition etc.[50]

The simplest node of the network, called the neuron, has several inputs and one output. The neuron sums the input values of x_j, each with its own weight w_j, and then transforms the result with a nonlinear activation function F.

$$y = F\left(\sum_{j=0}^{N} x_j w_j\right), x_0 \equiv 1$$

Neurons, differing from each other only by weight coefficients, are combined into blocks forming ANN layers.[50] An ANN is determined by the topology of the connection and the characteristics of the neurons, as well as by the learning algorithm. The most common topology, called the multilayer perceptron (MLP), was used in this study. In the MLP, the output of each neuron of the preceding layer is connected to the input of each neuron of the next layer (Figure 1).

The first layer of an MLP is called the input layer; the number of neurons in it is equal to the number of input features (here, spectrum channels) describing one pattern. Neurons of the input layer just distribute the input signal to all the neurons of the next layer. The last layer of an MLP is called the output layer; the number of neurons in it is the same as the number of parameters simultaneously determined in the given problem. The layers between the input and output layers are called hidden layers.

The application of ANN for solving inverse problems of optical spectroscopy is possible using several approaches.[40] The present study was conducted within the "experiment-based" approach, because there is no adequate analytical or numeric

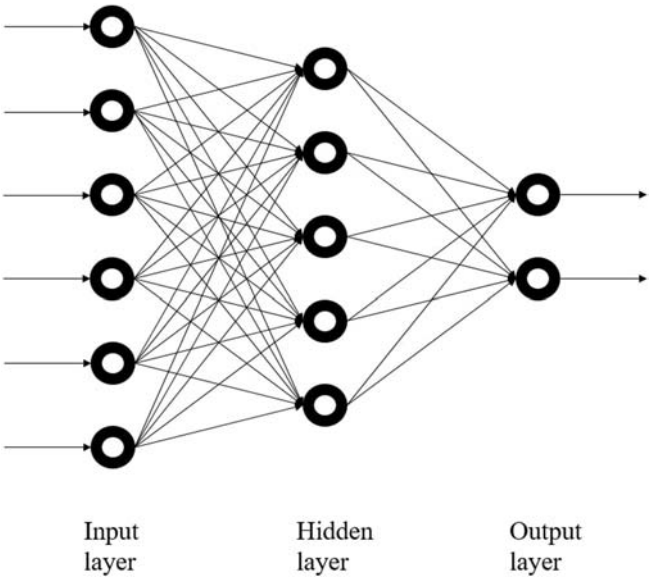

Figure 1. A scheme of the most common architecture of ANN — multilayer perceptron.

model describing the fluorescence intensity in each spectral channel as a function of the determined parameters (concentrations of different nanoparticles). In this approach, ANN is trained on experimental data. The disadvantage of this approach is that obtaining a large enough amount of experimental material is expensive and time consuming. The main advantage is that training ANN directly on the experimental data takes into account all molecular interactions and real experimental noise, thus increasing the accuracy of the solution of inverse problems.

The first stage of using ANN is its training on the known data patterns (training set). Training consists in changing the network weights in such a way that the error at the output of the network decreases. The most common algorithm for training the perceptron is the error back propagation algorithm.[50] One training event consists of sending a signal to the network inputs, obtaining output values, comparing them with the expected result in order to calculate the error, and sending the error back to the network to adjust the weight coefficients. Initially, the weights are initialized by random values.

The validation set is created in such a way that its patterns do not intersect with the patterns of the training set. It is used for periodic validation of the network during the training process in order to determine the moment of termination of the training and to prevent network overtraining. The network training is terminated when the average network error on the validation set does not decrease during a given number of training events.

To estimate the errors of the parameters determined in the problem being solved on independent data, an examination set is used. All the results presented below are those obtained on the examination set.

The quality of the ANN solution significantly depends on the input dimension of the problem. Not all input features are equally informative, and neural network architecture with a large number of input features has a very large number of weight coefficients. In this case, decreasing the number of input features can lead to an improvement in the neural net approximation. In this case, essential input features should be selected in an objective manner, rather than manually. In this paper, several algorithms were used to select the significant input features.

Results

Preparation and characterization of synthesized nanocomposites and their suspensions

Synthesized nGO was coated with PEG-PEI copolymers conjugated to FA by methods developed by the authors in Ref.[14, 51] (Figure 2). As a result, nGO+Cop+FA nanocomposites were obtained. Owing to the copolymer, the resulting nanoparticles are highly dispersible, biocompatible and able to carry molecular agents (FA) on their surfaces.[14]

FA was chosen as ligand for the nanocomposites due to the following reason. FA is necessary for growth of new cells, including oncological ones.[52] Therefore, tumors of certain types of cancer have the expression of the membrane protein-alpha receptors for folic acid (FRα). FRα has high affinity for folic acid (folate). As a result, the tumor "actively" takes FA from the body, which is used for the tumor growth[52] (the receptors on healthy cells are not accessible from the blood circulation). In this regard, FA is a commonly used "generic" targeting ligand used for cancer therapy. Therefore, FA ligands were attached to the surface of the nanocomposites to introduce generic cancer cell affinity.

FA also has a structural relative, methotrexate (MTX) that is an antimetabolite of antifolate type and commonly used as chemotherapy agent, which is taken up by the same receptors as folate.[53] Owing to this property, MTX can be simultaneously exploited as targeting ligand and anticancer drug when conjugated to the surface of nanoparticles.[54] Since the conjugation protocol is exactly the same, FA in our present nanoparticle system could be flexibly interchanged to MTX should the drug effect be desired to be exploited as well. A range of other drug compounds could also be attached to the polymeric surface coating utilizing the same coupling chemistry, which prevents the drug from being metabolized or released during delivery;[55] along with separate targeting ligands if desired.

The results of DLS measurement of sizes of all samples and the values of their zeta-potentials in HEPES buffer are shown in Table 1.

As follows from Table 1, dispersibility of nGO coated with copolymer and FA substantially increases. This is confirmed by the results obtained using transmission electron microscopy (TEM) (Figure 1 in Ref.[14]). The sizes of individual nGO+Cop and nGO+Cop+FA particles, determined from the TEM images after evaporation of the suspension, were about 10 nm. Therefore, coating of nGOs with copolymer and FA significantly reduces their aggregation, which is observed in their initial suspension at the concentration of 1 g/L.

To compare fluorescent properties of the initial nGOs and their nanocomposites, the fluorescence and Raman spectra of aqueous suspensions of nGO, nGO+Cop and nGO+Cop+FA were obtained at the concentration of 0.01 g/L (Figure 3). A narrow band with a maximum at 470 nm is the stretching band of

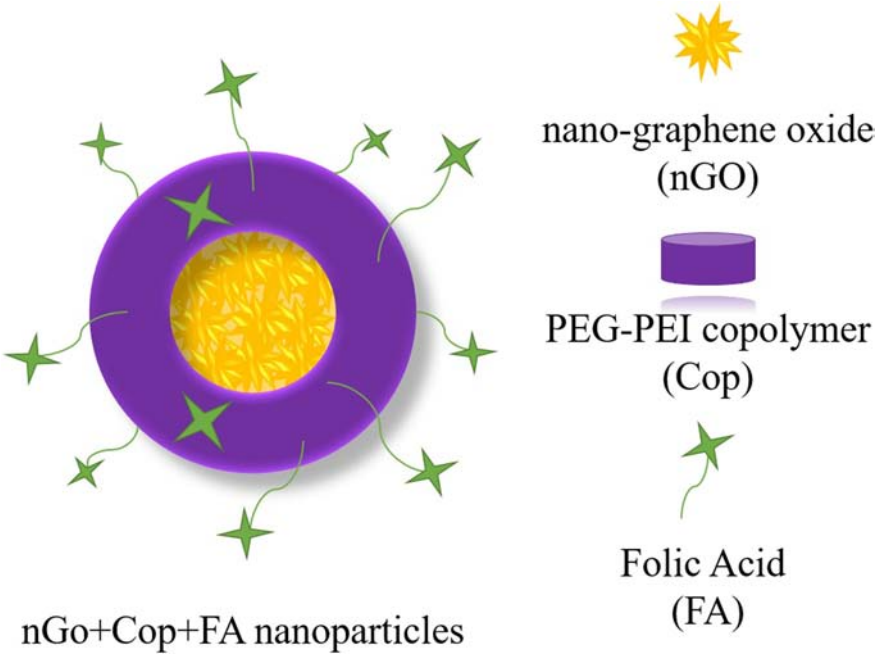

Figure 2. Schematic representation of synthesized nanocomposites and their components.

Table 1
Hydrodynamic radius and ζ-potential of nanocomposites and their components in HEPES buffer (25 mM, pH = 7.2) at the concentration of 1 g/L.

Sample	Size, nm	PDI	ζ-potential, mV
nGO	114 ± 2	0.287	−22.5 ± 0.3
nGO+Cop	34 ± 2	0.32	13.7 ± 0.3
nGO+Cop+FA	28 ± 1	0.34	−4.6 ± 0.6

water molecules, and a wide band from 410 to 700 nm is the fluorescence spectrum of the nanoparticles. The stretching band remains unchanged for all suspensions; therefore it is an internal benchmark in the study of fluorescence.

As can be seen from Figure 3, the maximum of fluorescence is shifted to the long-wavelength region as the initial nGO is covered with copolymer and FA (Table 2). The parameter F_0 was used for quantitative characterization of the fluorescence intensities of the samples. F_0 is the ratio of the integral intensity of fluorescence to the integral intensity of water Raman stretching band[56] (Figure 3). The values of the measured quantum yields and fluorescence parameters F_0 of all samples in water are shown in Table 2.

Comparative analysis of measured quantum yields and F_0 parameters shows that the coating of nGO with copolymer and FA does not cause fluorescence quenching of nanoparticles in water, but, on the contrary, slightly increases its intensity.

Evaluation and analysis of the biocompatibility of each of the nGO, nGO+Cop and nGO+Cop+FA samples against HeLa cancer cells showed that the viability of cells from the control group (without incubated nanocomposites) and cells with incubated nanoparticles was the same for all cells.[15] It was demonstrated that nGO and their nanocomposites at concentrations of 1 μg/mL, 10 μg/mL and 100 μg/mL are safe for cells.[14]

The possibility of visualization of nGO nanocomposites in HeLa cells using confocal fluorescence microscopy was demonstrated. Cancer cells were grown in a cell media containing nGO+Cop+FA for 7 h. Bright fluorescence of the nanocomposites in the cells was detected with confocal microscopy (exc. 488 nm) (Figure 4). It was found that nanoparticles are evenly distributed even inside daughter cells after cell division and provide visualization of cells for about a week, and FA ligands on the surface of nanocomposites increase the affinity to cancer cells.[14]

Thus, characterization of nGO, nGO+Cop and nGO+Cop +FA, carried out earlier[14] and at the present stage, shows that coating of nGO with copolymer and FA substantially increases dispersibility of nGO, slightly enhances the fluorescence properties of nanocomposites in comparison with initial nGO, and provides a good biocompatibility of nanoparticles and reliable visualization of them in cells *in vitro*. This means that the new nGO-synthesized nanocomposites are promising medical nanoagents.

Application of ANN to the solution of the problem of controlling the excretion of nanocomposites and their components from the body with urine

The task of monitoring the removal of nGO+Cop+FA and their components from the organism with urine by the fluorescence spectra was solved on model samples. The urine diluted 10 times was mixed with nGO+Cop+FA and its components in known quantities and various combinations, their fluorescence spectra were recorded and analyzed, and then neural network technologies were used. In this study, the

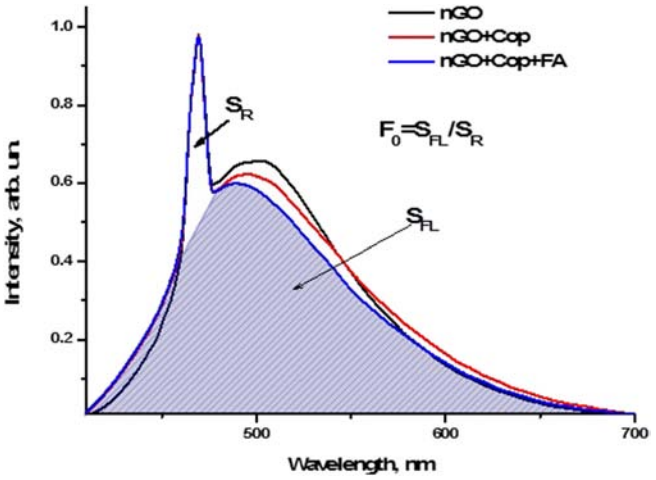

Figure 3. Fluorescence spectra of aqueous suspensions of nGO, nGO+Cop and nGO+Cop+FA at the concentration of 0.01 g/L. The spectra are normalized to the maximum intensity of the water Raman stretching band. Illustration of F_0 parameter calculation. S_R is the integral intensity of Raman stretching water band, S_{FL} is the integral intensity of nanoparticles fluorescence.

problems of determining the presence of a certain particles in urine and of determining the concentration of detected nanoparticles in urine were solved simultaneously using ANN, within the "experiment-based" approach.

Preliminary studies of the integrity of nGO+Cop+FA nanocomposites in suspensions with a change in pH from 5 to 8 showed that nGO+Cop+FA, nGO+Cop, and FA components are present in the suspensions. Therefore, a three-parameter inverse problem was solved to determine the presence and concentration of the most probable particles — nGO+Cop+FA, nGO+Cop and FA in urine. Of course, as a result of unloading and full assimilation of FA, it may be not present in urine. However, in this study, we demonstrate the principle possibility of determining its presence in urine in case of FA excess in the body.

Suspensions of nanoparticles with all possible 8 combinations of classes {nGO+Cop+FA}, {nGO+Cop}, {FA}, {nGO+Cop +FA, nGO+Cop}, {nGO+Cop+FA, FA}, {nGO+Cop, FA}, {nGO+Cop+FA, nGO+Cop, FA}, {urine without nanoparticles} were prepared in urine from three donors in the range of concentrations of each component from 0 to 2.15 mg/L.

Fluorescence spectra of all prepared samples were recorded with laser spectrometer (exc. 405 nm) in the range 400-800 nm. Each spectrum contained 1785 channels. 1461 fluorescence spectra were obtained. The spectra are shown in Figure 5 and Figure S1-S4. The bands with maxima at 470 nm are the Raman stretching bands of OH groups. Wide bands with maxima in the region of 520 nm are spectra of the superposition of urine fluorescence and fluorescence of nanoparticles.

Processing of the obtained spectra consisted in subtraction of the pedestal, which appears due to elastic light scattering, normalization to the spectral sensitivity of the device, and normalization of the spectra by the area of stretching vibrations of OH groups of urine.

The whole obtained array of data was divided into training, validation, and examination sets according to the ratio of

Table 2
Characterization of fluorescence properties of aqueous suspensions of nGO and its composites (the concentration is 0.01 g/L).

Parameter	GO	nGO+Cop	nGO+Cop+FA
Maximum of the fluorescence band, nm	92	497	502
F_0	15.8	16.1	17.0
Quantum yield of fluorescence, %	4.8	6.2	7.1

70:20:10, respectively. Thus, in the training set there were 991 patterns (spectra); in the validation set, 300 patterns; in the examination set, 168 patterns.

First, ANNs were trained on the full set of features (1785 channels). The following architectures of MLP were used: with one hidden layer, N01 (with 8, 16, 32 and 64 neurons in the hidden layer); with two hidden layers, N02 (with (8+4), (16+8), (32+16), (64+32) neurons in the hidden layers). The results of their application were averaged over 5 identical neural networks to reduce the influence of the initial weight coefficients values.

All ANN architectures had 3 outputs. The first output corresponded to the class nGO+Cop+FA, the second output – to nGO+Cop, the third output – to FA.

The results obtained using all the ANN architectures are presented in Table S1. Two-layer perceptron with 8 and 4 neurons in the hidden layers (N02(8+4)) provided the best mean absolute error of determining the concentration of nanoparticles on the examination set: 0.29 mg/L for nGO+Cop+FA, 0.44 mg/L for nGO+Cop, 0.47 mg/L for FA. This is 13.5% for nGO+Cop +FA, 20.5% for nGO+Cop, 21.9% for FA from the maximum content of nanoparticles in urine.

In order to reduce the input dimensionality of the problem and possible ANN overtraining, 4 alternative procedures for selection of significant input features were carried out: by cross-correlation and by cross-entropy between the values in each spectral channel and the values of each output, by standard deviation of the values in each spectral channel, and by neural network weight analysis. The procedures are described in Ref.[57] and in Supplementary material.

For comparison of the efficiency of the methods of selection, using each of them, the sets with about 500, about 1000 and about 1500 significant input features were formed.

The results of determining the concentrations of nanocomposites and their components in urine, obtained with (N02(8+4)) on the examination sets with selected input features, are presented in Table S2. The best result was obtained with the indicated ANN architecture on a set with 1000 significant input features that were selected by calculating the standard deviation (Figure 6).

Thus, the mean absolute error of determination of nanoparticles concentration on the examination set was 0.26 mg/L for nGO+Cop+FA, 0.41 mg/L for nGO+Cop, 0.45 mg/L for FA. This is 12.1% for nGO+Cop+FA, 19.1% for nGO+Cop, 20.9% for FA relative to the maximum content of nanoparticles in urine.

Comparative analysis of the obtained mean absolute errors of determination of the nanoparticles concentration in urine during training on the full set of features and on the dataset with only selected features showed that the selection procedure allowed us

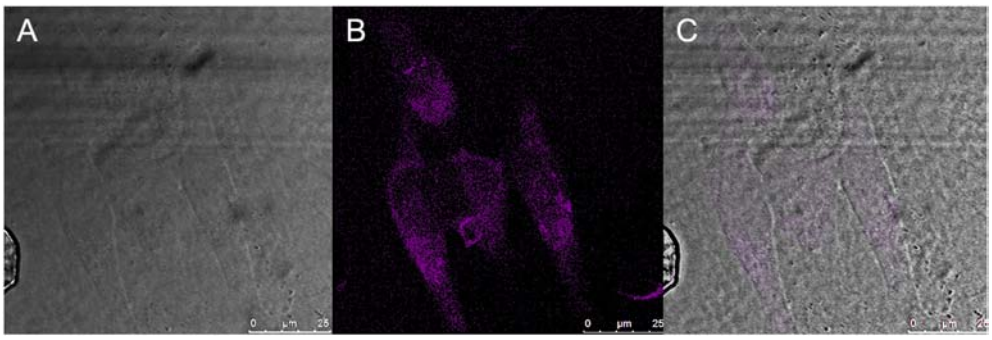

Figure 4. Fluorescence images from fixed HeLa cells incubated with 10 μg/mL of nanocomposite nGO+Cop+FA for 7 h: **(A)** bright field, **(B)** fluorescence, **(C)** overlay. Confocal imaging: argon laser Ex. 488 nm, Em. 520-580 nm.

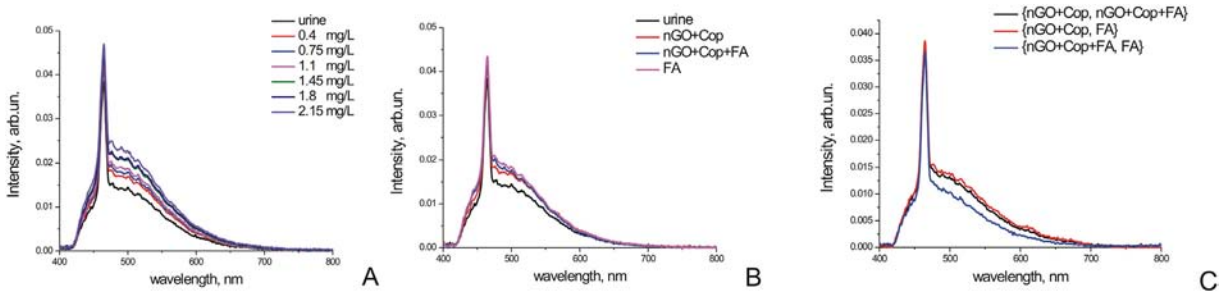

Figure 5. Fluorescence spectra of **(A)** urine, nGO+Cop+FA with various concentrations in urine; **(B)** urine, nGO+Cop+FA and their components with concentration of 2.15 mg/L in urine; **(C)** two-component suspensions of nanoparticles in urine with the following concentrations: 1.8 mg/L of {nGO+Cop, nGO +Cop+FA}; 2.15 mg/L of {nGO+Cop, FA}, 1.45 mg/L of {nGO+Cop+FA, FA}.

to increase the accuracy of the concentration determination by 7%.

It should be noted that the obtained accuracy of determining the concentration of deduced nanoparticles is given for the maximum content of nanoparticles in urine 2.15 mg/L. In practice, this content may be much more. For example, the authors of Ref.[17] created graphene oxide-based, sodium alginate functionalized colon-targeting drug delivery system, that is loaded with 5-fluorouracil as the anti-cancer drug and showed that this nanocomposite significantly inhibited tumor growth of mice. In these studies, in the blood of mice the nanocomposite suspension was injected from calculation of 3 mg per kg of body weight. If these values are extrapolated to the circulatory system of a person weighing 70 kg (approximately 5 L of blood), then we obtain the maximum content of nanocomposites in the blood 42 mg/L.

Discussion

The obtained results of the ANN application to the problem of monitoring the excretion of nanocomposites and their components from the organism with urine showed the wide possibilities of ANN methods. Several approaches can be distinguished even to the specific problem stated in this study:

1. If it is necessary to perform a quick estimation of the possibilities to determine the concentrations of all classes of nanoparticles in urine, it is advisable to use one ANN architecture that demonstrates the best result, averaged over all classes of substances. Improving the results is possible by selecting significant input features. This approach was implemented in this study.
2. In case it is necessary to determine the concentrations of all classes of nanoparticles in urine with very high accuracy, then, in order to identify each class of particles, one should use a certain single-output ANN architecture, “individual” for this class, — and apply a certain procedure for selecting significant input features. The time spent on obtaining the result will be proportional to the number of classes of substances in the investigated solution.
3. Increase in the number of experimental spectra may allow increasing the number of hidden layers and/or neurons in the hidden layers. In its turn, this may improve the results — reduce further the errors of determination of concentrations of nanocomposites and their components.

Thus, in this study a new approach to the implementation of optical imaging of luminescent nanoparticles in a biological medium using ANN is proposed. It has been demonstrated that simultaneous detection of nGO+Cop+FA, nGO+Cop, FA

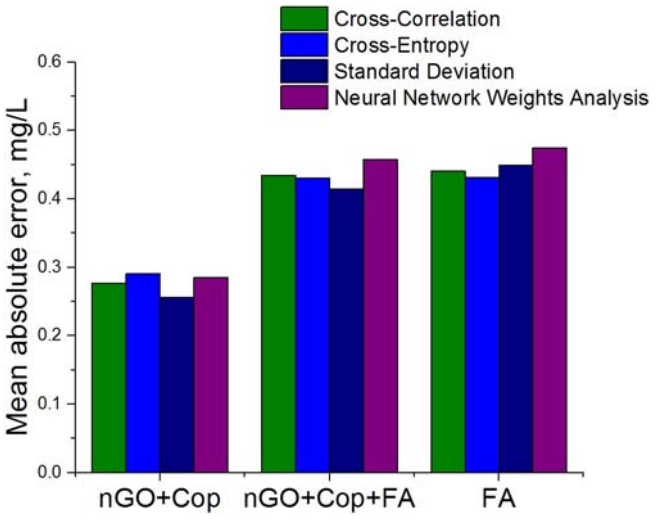

Figure 6. Mean absolute errors of determination of nGO+Cop+FA, nGO +Cop, FA in urine, obtained with (N02(8+4)) on the examination set with 1000 input features selected by various methods.

fluorescence against the background of the autofluorescence of human urine with a sufficiently low detection threshold of concentration not exceeding 12.1% for the nanocomposite nGO +Cop+FA, 19.1% for nGO+Cop, 20.9% for FA from the maximum content of nanoparticles is possible with the help of ANNs.

It is necessary to note the following advantages and prospects of the proposed method of visualization of nanoparticles in biological tissues.

In our case of using fluorescence spectroscopy, obtaining a set of experimental data requires fairly simple and cheap equipment. Obviously, one can work with skin, blood, urine, near-surface vessels in this way. It is not yet possible to obtain a fluorescent signal from the deep layers of the biological system, but only from the slices. Nevertheless, the developed method can be applied to excite signals, for example, using X-ray sources, in case it is possible to excite and receive a signal from the depth of the biosystem.

The fact that training of neural networks takes into account all possible interactions of nanoparticles with biomacromolecules is an important advantage of using ANN. Of course, here working with specific nanoparticles and a specific biological object is meant. For another biosystem and other nanoparticles, ANN training should be repeated anew on the appropriate experimental datasets. In this study, three-parameter inverse problem of fluorescence spectroscopy was solved, using ANN: three classes of nanoparticles were identified. Similarly, problems with a larger number of parameters, nanoparticle classes, can be solved.

Thus, the example of a successful solution of the problem of monitoring the removal of nanocomposites based on nGO and their components with urine using ANN demonstrated the possibility of solving complex multi-parameter inverse problems of imaging luminescent nanoparticles in biological tissues. This approach can be used for detection and quantitative evaluation of the content of various types of luminescent nanoparticles – both diagnostic and therapeutic – in blood, various organs, in the cells.

Appendix A. Supplementary data

Supplementary data to this article can be found online at https://doi.org/10.1016/j.nano.2018.03.009.

References

1. Ferlay J, Soerjomataram I, Dikshit R, Eser S, Mathers C, Rebelo M, et al. Cancer incidence and mortality worldwide: sources, methods and major patterns in GLOBOCAN 2012. *International Journal of Cancer* 2015;**136**(5), https://doi.org/10.1002/ijc.29210.
2. Torre LA, Siegel RL, Ward EM, Jemal A. Global cancer incidence and mortality rates and trends—an update. *Cancer Epidemiol Prevent Biomark* 2016;**25**(1):16-27, https://doi.org/10.1158/1055-9965 [EPI-15-0578].
3. Jones SK, Merkel OM. Tackling breast cancer chemoresistance with nano-formulated siRNA. *Gene Ther* 2016;**23**(12):821, https://doi.org/10.1038/gt.2016.
4. Arranja AG, Pathak V, Lammers T, Shi Y. Tumor-targeted nanomedicines for cancer theranostics. *Pharmacol Res* 2017;**115**:87-95, https://doi.org/10.1016/j.phrs.2016.11.014.
5. Lammers T, Aime S, Hennik WE, Storm G, Iessling F. Theranostic nanomedicine. *Acc Chem Res* 2011;**44**(10):1029-38, https://doi.org/10.1021/ar200019c.
6. Massoud TF, Gambhir SS. Molecular imaging in living subjects: seeing fundamental biological processes in a new light. *Genes Dev* 2003;**17**(5):545-80, https://doi.org/10.1101/gad.1047403.
7. Janib SM, Moses AS, MacKay JA. Imaging and drug delivery using theranostic nanoparticles. *Adv Drug Deliv Rev* 2010;**62**(11):1052-63, https://doi.org/10.1016/j.addr.2010.08.004.
8. Beer AJ, Schwaiger M. Imaging of integrin αvβ3 expression. *Cancer Metastasis Rev* 2008;**27**(4):631-44, https://doi.org/10.1007/s10555-008-9158-3.
9. Mody VV, Nounou MI, Bikram M. Novel nanomedicine-based MRI contrast agents for gynecological malignancies. *Advanced Drug Delivery Reviews* 2009;**61**(10):795-807, https://doi.org/10.1016/j.addr.2009.04.020.
10. Jenkins R, Burdette MK, Foulger SH. Mini-review: fluorescence imaging in cancer cells using dye-doped nanoparticles. *RSC Adv* 2016;**6**(70):65459-74, https://doi.org/10.1039/C6RA10473H.
11. Zhou Y, Jing X, Chen Y. Material chemistry of graphene oxide-based nanocomposites for theranostic nanomedicine. *J Mater Chem B* 2017;**5**:6451-70, https://doi.org/10.1039/C7TB00680B.
12. Wu Y, Ermakova A, Liu W, Pramanik G, Vu TM, Kurz A, et al. Programmable biopolymers for advancing biomedical applications of fluorescent nanodiamonds. *Adv Funct Mater* 2015;**25**(42):6576-85, https://doi.org/10.1002/adfm.201502704.
13. Zhang L, Lu Z, Zhao Q, Huang J, Shen H, Zhang Z. Enhanced chemotherapy efficacy by sequential delivery of siRNA and anticancer drugs using PEI-grafted graphene oxide. *Small* 2011;**7**(4):460-4, https://doi.org/10.1002/smll.201001522.
14. Prabhakar N, Näreoja T, von Haartman E, Karaman DŞ, Burikov SA, Dolenko TA, et al. Functionalization of graphene oxide nanostructures improves photoluminescence and facilitates their use as optical probes in preclinical imaging. *Nanoscale* 2015;**7**(23):10410-20, https://doi.org/10.1039/c5nr01403d.
15. Zhang B, Yan Y, Shen Q, Ma D, Huang L, Cai X, et al. A colon targeted drug delivery system based on alginate modificated graphene oxide for colorectal liver metastasis. *Mater Sci Eng C* 2017;**79**:185-90, https://doi.org/10.1016/j.msec.2017.05.054.

16. Aldeek F, Muhammed MH, Palui G, Zhan N, Mattoussi H. Growth of highly fluorescent polyethylene glycol-and zwitterion-functionalized gold nanoclusters. *ACS Nano* 2013;**7**(3):2509-21, https://doi.org/10.1021/nn305856t.
17. Bartelmess J, Quinn SJ, Giordani S. Carbon nanomaterials: multi-functional agents for biomedical fluorescence and Raman imaging. *Chem Soc Rev* 2015;**44**(14):4672-98, https://doi.org/10.1039/c4cs00306c.
18. Rao J, Dragulescu-Andrasi A, Yao H. Fluorescence imaging in vivo: recent advances. *Curr Opin Biotechnol* 2007;**18**(1):17-25, https://doi.org/10.1016/j.copbio.2007.01.003.
19. Zellweger M. Autofluorescence of the human bronchial tissue. Fluorescence spectroscopy of exogenous, exogenously-induced and endogenous fluorofores for the photodetection and photodynamic therapy of cancer. *Lausanne* 2000:117-43.
20. Demchenko AP. Organic dyes. *Introduction to fluorescence sensing*. Springer Science & Business Media; 2008. p. 119-44.
21. Kim S, Fisher B, Eisler HJ, Bawendi M. Type-II quantum dots: CdTe/CdSe (core/shell) and CdSe/ZnTe (core/shell) heterostructures. *J Am Chem Soc* 2003;**125**(38):11466-7, https://doi.org/10.1021/ja0361749.
22. Bogdanov KV, Osipov VY, Zhukovskaya MV, Jentgens C, Treussart F, Hayashi T, et al. Size-dependent Raman and SiV-center luminescence in polycrystalline nanodiamonds produced by shock wave synthesis. *RSC Adv* 2016;**6**(57):51783-90, https://doi.org/10.1039/C6RA09317E.
23. Choi S, Kim P, Boutilier R, Kim MY, Lee YJ, Lee H. Development of a high speed laser scanning confocal microscope with an acquisition rate up to 200 frames per second. *Opt Express* 2013;**21**(20):23611-8, https://doi.org/10.1364/OE.21.023611.
24. Helmchen F, Denk W. New developments in multiphoton microscopy. *Curr Opin Neurobiol* 2002;**12**(5):593-601, https://doi.org/10.1016/S0959-4388(02)00362-8.
25. Suhling K, French PM, Phillips D. Time-resolved fluorescence microscopy. *Photochem Photobiol Sci* 2005;**4**(1):13-22, https://doi.org/10.1039/b412924p.
26. Xu M, Wang LV. Photoacoustic imaging in biomedicine. *Rev Sci Instrum* 2006;**77**(4):041101, https://doi.org/10.1063/1.2195024.
27. Burns AA, Vider J, Ow H, Herz E, Penate-Medina O, Baumgart M, et al. Fluorescent silica nanoparticles with efficient urinary excretion for nanomedicine. *Nano Letts* 2008;**9**(1):442-8, https://doi.org/10.1021/nl803405h.
28. Balogh L, Nigavekar SS, Nair BM, Lesniak W, Zhang C, Sung LY, et al. Significant effect of size on the in vivo biodistribution of gold composite nanodevices in mouse tumor models. *Nanomedicine* 2007;**3**(4):281-96, https://doi.org/10.1016/j.nano.2007.09.001.
29. Galanzha EI, Shashkov EV, Spring PM, Suen JY, Zharov VP. In vivo, noninvasive, label-free detection and eradication of circulating metastatic melanoma cells using two-color photoacoustic flow cytometry with a diode laser. *Cancer Res* 2009;**69**(20):7926-34, https://doi.org/10.1158/0008-5472.CAN-08-4900.
30. van de Linde S, Heilemann M, Sauer M. Live-cell super-resolution imaging with synthetic fluorophores. *Annu Rev Phys Chem* 2012;**63**:519-40, https://doi.org/10.1146/annurev-physchem-032811-112012.
31. Coraluppi S, Carthel C. Multi-stage multiple-hypothesis tracking. *J Adv Inf Fusion* 2011;**6**(1):57-67, https://pdfs.semanticscholar.org/c8a8/c2f572bf55e11f068f684b2dfeaf9958356c.pdf.
32. Dupont A, Lamb DC. Nanoscale three-dimensional single particle tracking. *Nanoscale* 2011;**3**(11):4532-41, https://doi.org/10.1039/c1nr10989h.
33. Manzo C, Garcia-Parajo MF. A review of progress in single particle tracking: from methods to biophysical insights. *Rep Prog Phys* 2015;**78**(12):124601, https://doi.org/10.1088/0034-4885/78/12/124601.
34. von Diezmann A, Shechtman Y, Moerner WE. Three-dimensional localization of single molecules for super-resolution imaging and single-particle tracking. *Chem Rev* 2017;**117**:7244-75, https://doi.org/10.1021/acs.chemrev.6b00629.
35. Hassoun MH. Computational capabilities of artificial neural networks. *Fundamentals of Artificial Neural Networks*. 1st ed. Cambridge, USA: MIT Press; 1995. p. 35-45.
36. Keedwell E, Narayanan A. *Neural Networks. Intelligent Bioinformatics: The Application of Artificial Intelligence Techniques to Bioinformatics Problems*. Chichester, England: John Wiley & Sons Ltd; 2005173-93.
37. Chervonenkis AY. Application of methods of pattern recognition in problems of molecular biology. *Probl Manage* 2005;**4**:41-6.
38. Lenhardt L, Zeković I, Dramićanin T, Dramićanin MD. Artificial neural networks for processing fluorescence spectroscopy data in skin cancer diagnostics. *Phys Scr* 2013;**2013**(T157):014057, https://doi.org/10.1088/0031-8949/2013/T157/014057.
39. Li MM, Verma B, Fan X, Tickle K. RBF neural networks for solving the inverse problem of backscattering spectra. *Neural Comput Appl* 2008;**17**(4):391-7, https://doi.org/10.1007/s00521-007-0138-2.
40. Gerdova IV, Dolenko SA, Dolenko TA, Churina IV, Fadeev VV. New opportunity solutions to inverse problems in laser spectroscopy involving artificial neural networks. *Izv Akad Nauk Ser Fiz* 2002;**66**(8):1116-24.
41. Dolenko SA, Gerdova IV, Dolenko TA, Fadeev VV. Laser fluorimetry of mixtures of polyatomic organic compounds using artificial neural networks. *Quantum Electron* 2001;**31**(9):834.
42. Dolenko SA, Dolenko TA, Fadeev VV, Gerdova IV, Kompitsas M. Time-resolved fluorimetry of two-fluorophore organic systems using artificial neural networks. *Opt Commun* 2002;**213**(4):309-24, https://doi.org/10.1016/S0030-4018(02)02078-3.
43. Shalaby KS, Soliman ME, Casettari L, Bonacucina G, Cespi M, Palmieri GF, et al. Determination of factors controlling the particle size and entrapment efficiency of noscapine in PEG/PLA nanoparticles using artificial neural networks. *Nanomedicine* 2014;**9**:4953, https://doi.org/10.2147/IJN.S68737.
44. Baharifar H, Amani A. Cytotoxicity of chitosan/streptokinase nanoparticles as a function of size: an artificial neural networks study. *Nanomedicine* 2016;**12**(1):171-80, https://doi.org/10.1016/j.nano.2015.09.002.
45. Houška J, Peña-Méndez EM, Hernandez-Fernaud JR, Salido E, Hampl A, Havel J, et al. Tissue profiling by nanogold-mediated mass spectrometry and artificial neural networks in the mouse model of human primary hyperoxaluria 1. *J Appl Biomed* 2014;**12**(2):119-25, https://doi.org/10.1016/j.jab.2013.12.001.
46. Dolenko TA, Burikov SA, Vervald AM, Vlasov II, Dolenko SA, Laptinskiy KA, et al. Optical imaging of fluorescent carbon biomarkers using artificial neural networks. *J Biomed Opt* 2014;**19**(11):117007.
47. Laptinskiy K, Burikov S, Dolenko S, Efitorov A, Sarmanova O, Shenderova O, et al. Monitoring of nanodiamonds in human urine using artificial neural networks. *Phys Status Solidi A* 2016;**213**(10):2614-22, https://doi.org/10.1002/pssa.201600178.
48. Ciftan Hens S, Lawrence WG, Kumbhar AS, Shenderova O. Photoluminescent nanostructures from graphite oxidation. *J Phys Chem C* 2012;**116**(37):20015-22, https://doi.org/10.1021/jp303061e.
49. Magde D, Wong R, Seybold PG. Fluorescence quantum yields and their relation to lifetimes of rhodamine 6G and fluorescein in nine solvents: improved absolute standards for quantum yields. *Photochem Photobiol* 2002;**75**(4):327-34.
50. Haykin SS. Multilayer perceptron. In: Horton MJ, Dworkin A, Mars D, Disanno S, Dulles G, editors. *Neural Networks and Learning Machines*. 3rd ed. New Jersey, USA: Pearson; 2009. p. 123-221.
51. Karaman DŞ, Gulin-Sarfraz T, Hedström G, Duchanoy A, Eklund P, Rosenholm JM. Rational evaluation of the utilization of PEG-PEI copolymers for the facilitation of silica nanoparticulate systems in biomedical applications. *J Colloid Interface Sci* 2014;**418**:300-10, https://doi.org/10.1016/j.jcis.2013.11.080.
52. Kim YI. Role of folate in colon cancer development and progression. *J Nutr* 2003;**133**(11):3731S-9S.
53. Wibowo AS, Singh M, Reeder KM, Carter JJ, Kovach AR, Ratnam WMM, et al. Structures of human folate receptors reveal biological trafficking states and diversity in folate and antifolate recognition. *PNAS* 2013;**110**(38):15180-8, https://doi.org/10.1073/pnas.1308827110.

54. Rosenholm JM, Peuhu E, Bate-Eya LT, Eriksson JE, Sahlgren C, Lindén M. Cancer-cell-specific induction of apoptosis using mesoporous silica nanoparticles as drug-delivery vectors. *Small* 2010;**6**(11):1234-41, https://doi.org/10.1002/smll.200902355/full.
55. Santiago T, DeVaux RS, Kurzatkowska K, Espinal R, Herschkowitz JI, Hepel M. Surface-enhanced Raman scattering investigation of targeted delivery and controlled release of gemcitabine. *Nanomedicine* 2017;**12**:7763-76, https://doi.org/10.2147/IJN.S149306.
56. Dolenko TA, Burikov SA, Rosenholm JM, Shenderova OA, Vlasov II. Diamond–water coupling effects in Raman and photoluminescence spectra of nanodiamond colloidal suspensions. *J Phys Chem C* 2012;**116**(45):24314-9, https://doi.org/10.1021/jp306803n.
57. Efitorov A, Burikov S, Dolenko T, Laptinskiy K, Dolenko S. Significant feature selection in neural network solution of an inverse problem in spectroscopy. *Proc Comput Sci* 2015;**66**:93-102, https://doi.org/10.1016/j.procs.2015.11.012.